J. Micromech. Microeng. **17** (2007) 2516–2521 doi:10.1088/0960-1317/17/12/018

Fabrication of beam structures with micro-scale cross-sections and meso-scale spans

Michael James Martin[1,3], **Robert D White**[2,4], **Katsuo Kurabayashi**[2] **and Iain D Boyd**[1]

[1] Department of Aerospace Engineering, University of Michigan, Ann Arbor, MI, USA
[2] Department of Mechanical Engineering, University of Michigan, Ann Arbor, MI, USA

Received 18 September 2007, in final form 10 October 2007
Published 6 November 2007
Online at stacks.iop.org/JMM/17/2516

Abstract
To allow testing of micro-scale aerodynamics, a process was created to manufacture beam structures that combine spans of 1 cm with a cross-section of 5 μm by 100 μm. The structural considerations limiting the fabrication of a structure combining macro-scale spans with a micro-scale cross-section are analyzed. Limiting considerations include forces during operation, fluid forces during release, vibrational limitations and beam buckling. Based on these results, a fabrication process for creating a beam structure for large spans without support structures is devised, incorporating the use of back-side etches and extra handling wafers to avoid stiction. This process is used to successfully fabricate the desired structure.

(Some figures in this article are in colour only in the electronic version)

1. Introduction

There is growing engineering interest in flight at the micro- and nano-scales. Potential applications include battle-field surveillance, search-and-rescue operations and monitoring of hazardous materials [1]. As such devices are reduced in scale, the aerodynamics are complicated by the breakdown of the continuum assumption [2, 3]. Design at these scales requires the development both of new computational methods [4, 5] and of new methods for aerodynamic testing [6]. Measurement of air flows at these scales is much more challenging than measurement of liquid flows [7]. Current micro-PIV technology in air flows has a resolution of approximately 10 μm [8]. This increases the importance of indirect measurements, such as force measurements, in investigation of air flow at these scales. Computational results indicate that a measurable reduction in drag will occur as a result of rarefied flow effects [9, 10].

To allow integration with existing micro-scale aerodynamics facilities [6], a test configuration has been proposed in which a 1 cm span airfoil is suspended between two mounting plates as shown in figure 1. Microfabrication technology allows force sensors to be integrated into the mounting plates. However, to realize this configuration, a fabrication process must be developed to allow the creation of a flat-plate airfoil with a meso-scale span and a micron-scale cross-section. The present work analyzes the fabrication issues in creating this device, and demonstrates a process for the creation of micro-beams with micron-scale cross-sections and meso-scale spans.

2. Structural constraints

The maximum allowable design width of the beam used in testing is set by the expected force during testing. However, three sets of structural limitations affect the allowable length of a micro-fabricated beam structure: buckling during release, structural loading in liquid flow around the beam during release and possible low natural frequencies for the resulting beam structure. Each of these constraints is considered individually.

2.1. Aerodynamic drag

Structural considerations limit the maximum chord of any micro-scale airfoil and the width of the facility. The maximum

[3] Current address: Naval Research Laboratory, Washington, DC, USA.
[4] Current address: Department of Mechanical Engineering, Tufts University, Medford, MA, USA.

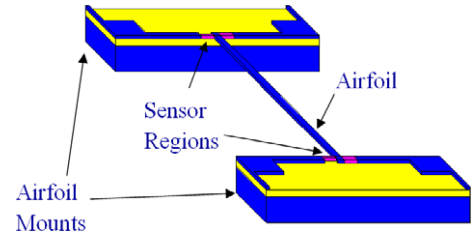

Figure 1. An integrated flat plate airfoil and sensor design.

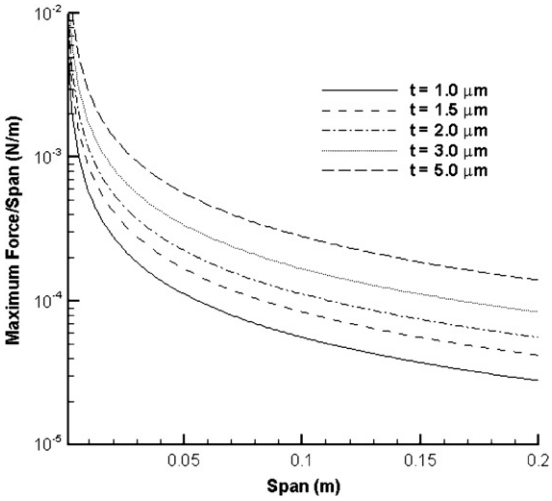

Figure 2. Allowable force/span versus span for a 100 μm airfoil.

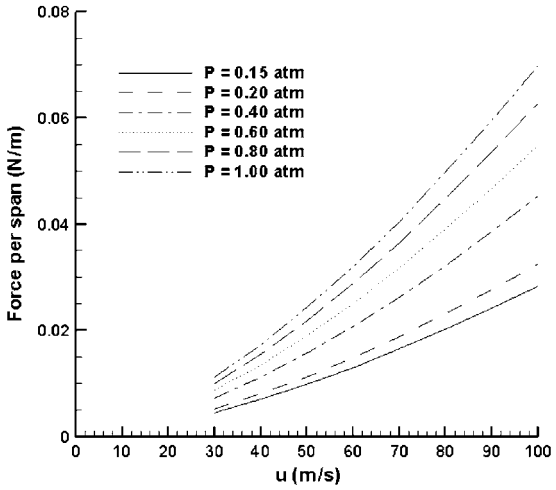

Figure 3. Drag force for per span, 100 μm chord airfoil.

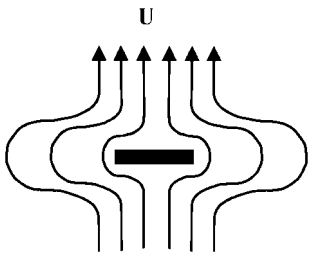

Figure 4. Flow around the beam during release.

allowable span of the airfoil is found by modeling the system as a beam under uniform loading [11]. In this case, the maximum stress seen in the airfoil will be at the end of the airfoil:

$$\sigma_{\max} = \frac{3Sf}{2c^3t}, \tag{1}$$

where $\sigma_{\max}$ is the maximum stress, S is the span of the beam, c is the chord, t is the thickness and f is the force per unit span.

Based on the mechanical properties of silicon [12], and a safety factor of 1.5, the maximum allowable force for 100 μm chord airfoils as a function of thickness and span is shown in figure 2.

These results can be compared to the aerodynamic forces for a 100 μm airfoil calculated using a modified boundary layer theory that incorporates non-equilibrium effects [9]. This theory is expected to give higher forces than what actually occur in testing, which makes its use a conservative assumption. A plot of the force per span as a function of velocity for pressures ranging from 0.1 to 1.0 atm is shown in figure 3. Comparing the maximum allowable forces in figure 2 to the expected aerodynamic forces in figure 3 allows the selection of a maximum allowable span for airfoil testing. Based on these concerns, a span of 1 cm was selected for airfoil testing.

2.2. Viscous drag during beam release

A similar analysis can be carried out to obtain the maximum allowable force on the beams during release. As the beam is pulled away from the support structure during release, the flow around the beam will create force on the beam. The flow geometry is shown in figure 4.

Low Reynolds number fluid flow theory [13] suggests that the force on the beam per unit span F_D will be a function of the beam width c, the fluid velocity U and the fluid viscosity μ:

$$\frac{F_D}{S} \propto U\mu c. \tag{2}$$

To calculate the expected fluid forces, a commercial computational fluid dynamics package was used [14]. The expected forces were calculated for a beam with a chord of 100 μm and a thickness of 5 μm for velocities ranging from 0.1 to 2.0 mm s^{-1}. Acetone is the usual release fluid to remove photoresist, but recent researchers have had success with fragile structures using pentane [15], which has a lower viscosity and surface tension [16]. The results are shown in figure 5. Figure 5 shows that the use of a low-viscosity fluid, when combined with low velocities during the release process, can substantially decrease the forces encountered during the release.

The allowable structural loads on the beam can be found by modeling the system as a beam under uniform loading [11]. In this case, the maximum stress seen in the airfoil will be at the end of the plate:

$$\sigma_{\max} = \frac{3Sf}{2t^3c}, \tag{3}$$

where $\sigma_{\max}$ is the maximum stress, S is the span of the beam, c is the chord, t is the thickness and f is the force per unit span.

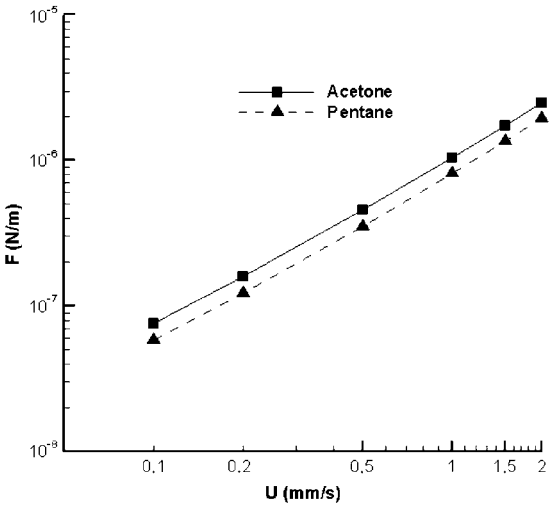

Figure 5. Expected viscous forces during release.

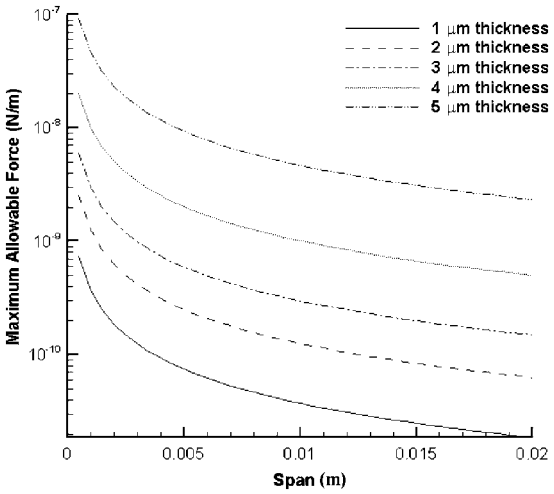

Figure 6. Maximum allowable force during release.

Using a factor of safety of 1.5, and the mechanical properties of crystalline silicon, the maximum allowable force during release on a beam with a chord of 100 μm is shown in figure 6. A comparison of figure 5 with figure 6 shows that, by using a low-viscosity fluid such as pentane, and a wet release process that minimizes fluid motion, it is possible to successfully release silicon beam structures with a chord of 100 μm, a thickness of 5 μm and a span of 1 cm.

2.3. Vibration

The first natural frequency of the first vibrational mode of a structure clamped at both ends is given by

$$\omega = \frac{4.73^2}{S^2} t \sqrt{\frac{E}{12\rho_{\text{beam}}}}, \tag{4}$$

where ω is the natural frequency, E is the elastic modulus and ρ_{beam} is the density of the beam [17]. Using the properties of crystalline silicon, figure 7 shows the natural frequency of a micro-machined silicon beam as a function of thickness and span.

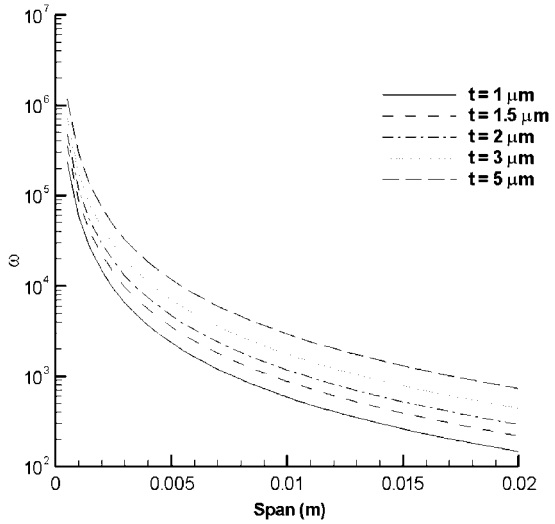

Figure 7. Natural frequency for a silicon beam as a function of span and thickness.

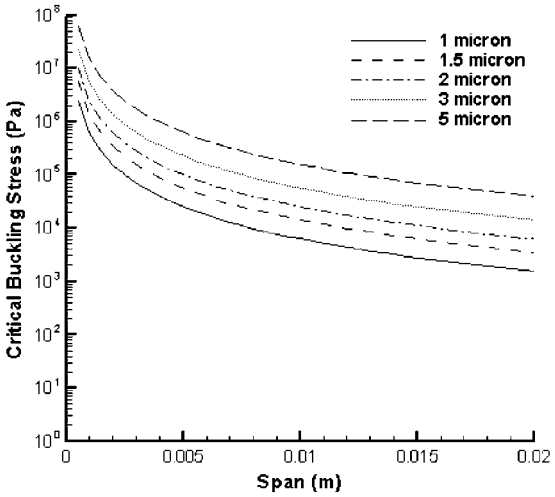

Figure 8. Critical buckling stress for a silicon beam as a function of span and thickness.

These results suggest that as the beam thickness approaches 1 μm, even low frequency vibrations within the fabrication process may excite the beam. Therefore, the process should be designed so that individual dies are separated without the use of a die saw.

2.4. Beam buckling

Buckling during release is encountered in a variety of MEMS applications [18]. Buckling in microstructures typically results from thermal stresses in the materials, usually as a result of deposition at high temperatures. The critical stress required to buckle a microbeam is given by

$$\sigma_{\text{crit}} = \frac{4\pi^2 EI}{S^2 A} = \frac{\pi^2 Et^2}{3S^2}, \tag{5}$$

where I is the moment of inertia of the beam cross-section and A is the beam cross-sectional area [18]. The critical stress for a silicon microbeam as a function of thickness and length is given in figure 8.

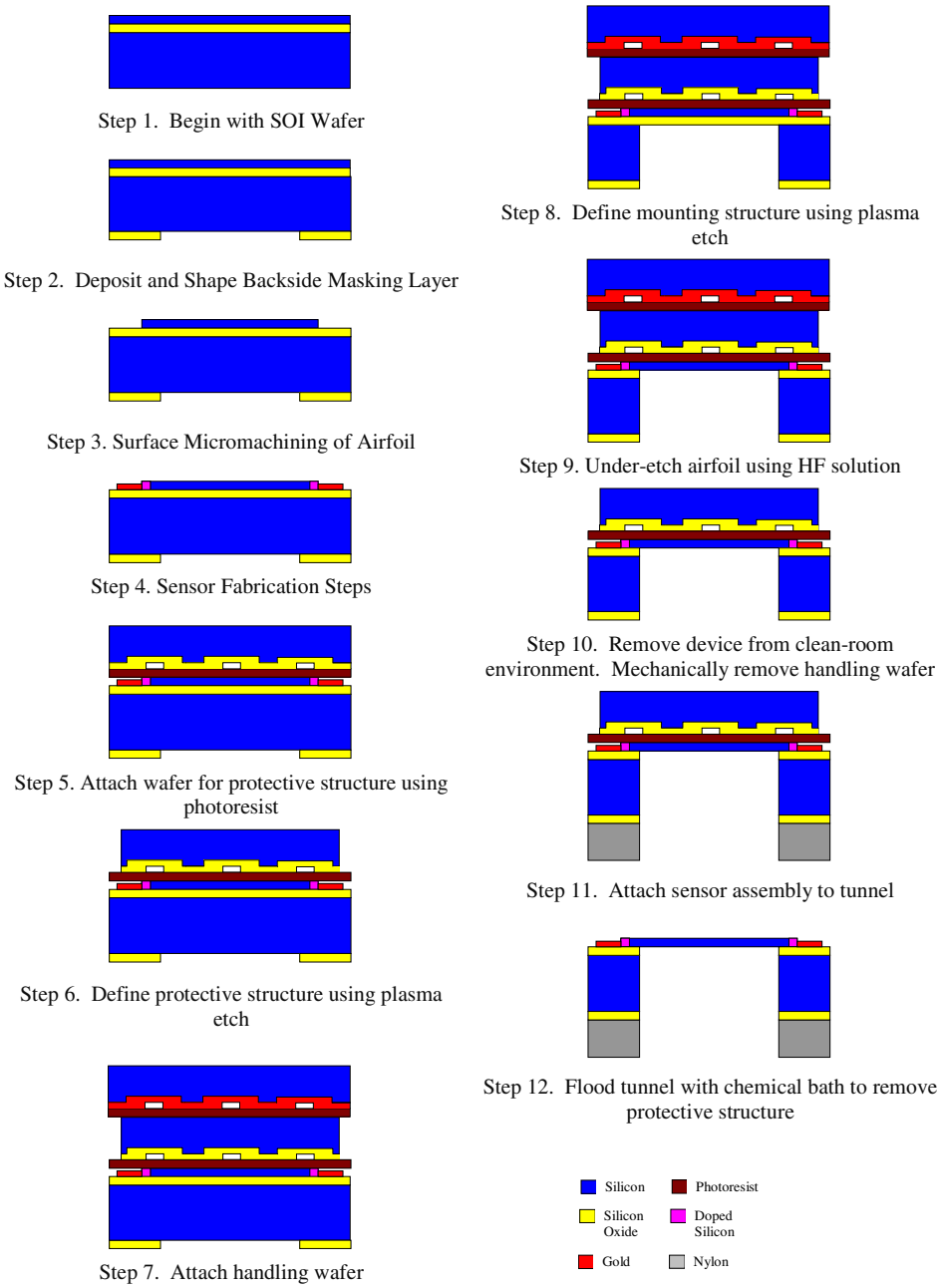

Figure 9. Process flow.

The build-up of thermal stress can be avoided by a careful selection of wafer materials. Silicon-on-insulator wafers using mechanically attached layers will have lower thermal stresses than wafers using oxide deposited at high temperatures, and should be used for this process.

All of these results suggest that for a micro-machined structure with a length on the order of mm or cm, the practical limit for thickness is on the order of 1 μm.

3. Fabrication process

Based on these constraints, a fabrication process was devised that allowed the installation of the beam structure with mounting plates in spanning a macro-scale channel. The process requires three wafers: an SOI wafer for fabrication of the device and two handle wafers. The two handle wafers are grooved with micro-channels using an RIE etch. The first handle wafer, which will be used to create protective plates, is coated with a silicon oxide layer to prevent stiction. The second handle wafer, which will be used to keep individual dies together during through-wafer etches, is coated with gold.

The complete fabrication process is shown in figure 9. The process begins with an SOI wafer, featuring a 5 μm device layer and a 2 μm buried oxide layer. The back of the wafer is then coated with a 5 μm thick oxide layer, which is then etched using an HF etch into the mask for the final mounting. This step avoids the presence of photoresist on the mounts during the final release. The airfoil shape is then defined using

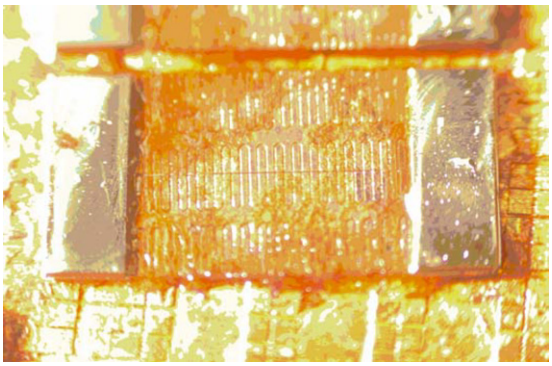

Figure 10. Device prior to mounting.

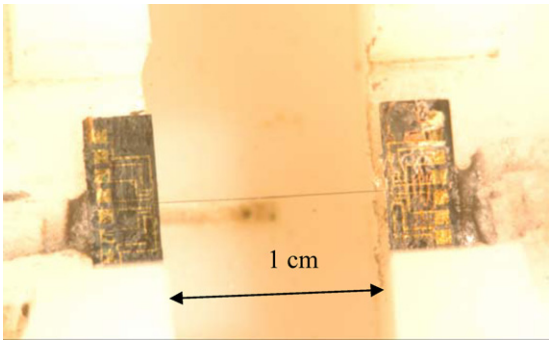

Figure 11. The released airfoil.

a plasma etch of the device layer. Any additional doping, wiring deposition or other steps needed to create force sensors are incorporated into the fabrication process at this point.

The first handle wafer is then attached and etched to form a protective structure, designed to support the airfoil and mounts during installation. The assembly is then mounted to the second handle wafer, which is designed to hold the individual dies together during the through-wafer etch.

The mounting structure is then defined using a deep plasma etch. This etch not only removes the silicon from underneath the airfoil, but also removes the material between the dies, eliminating the need for use of a die saw. A timed HF etch is then used to remove the oxide from underneath the airfoil. The resulting die is shown in figure 10.

After the die is mechanically removed from the handle wafer, the device is mounted into its final location using epoxy. The tunnel is first flooded with acetone to remove the photoresist, then with isopropanol and finally with pentane. The protective structure is removed using a mechanical lifter, leaving behind a free-standing airfoil, as shown in figure 11.

4. Results

After release, devices were examined using the FEI Quanta 200 3D focused ion beam environmental scanning electron microscope in low pressure. Figure 12 shows the mounting point where the beam joins the sensor region. This photograph shows that the beam retains its shape as it joins the mounting point. It also shows that the through-wafer etch required to release the backside of the beam overlaps the freestanding beam by approximately 100 μm. Because of the sacrificial oxide layer, the beam is still free standing in this area.

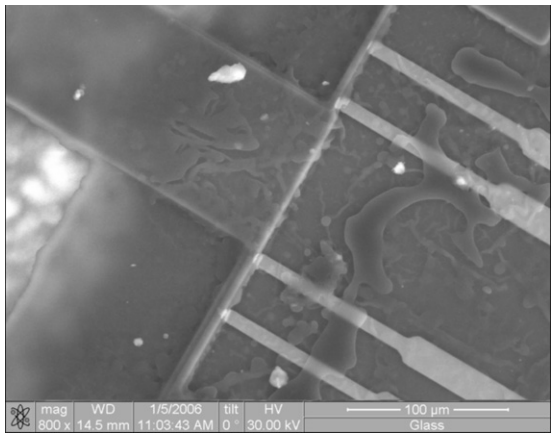

Figure 12. An electron microscope image of the mounting region.

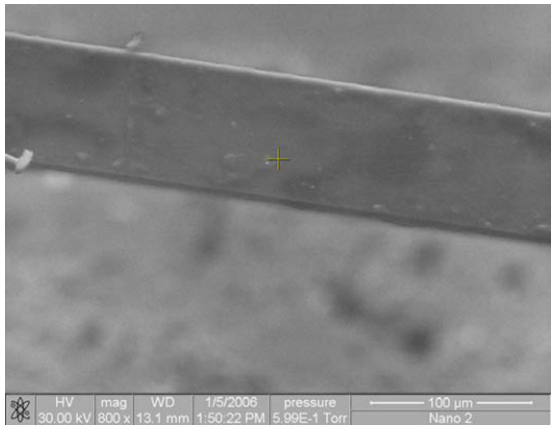

Figure 13. An electron microscope image of the airfoil structure.

Figure 13 shows the freestanding beam at a 35° angle. This photograph shows that the beam retains a rectangular cross-section during processing.

5. Conclusions

Based on the analysis of the forces acting on a micro-machined airfoil during the fabrication and release process, the limiting factors on the fabrication of micromachined beam structures of macroscopic length were identified as fluid forces during release, beam buckling and vibration. A fabrication process was devised which minimized the effect of all of these constraints. This required the use of a relatively elaborate fabrication process, which incorporated the use of two handle wafers and low-stress SOI wafers.

Adoption of this process allowed the fabrication of a 1 cm span flat-plate airfoil with a 5 μm by 100 μm rectangular cross-section. The fabrication process can be integrated with a variety of potential sensor configurations at the mounting location, allowing for the development of aerodynamic testing of micro-scale devices.

Acknowledgments

The authors gratefully acknowledge support for this work from the Air Force Office of Scientific Research through MURI grant no. F49620-98-1-043. The authors wish to thank the staff members of the Michigan Nanofabrication Facility, particularly Katherine Beach, Aaron Glatzer, Ning Gulari, Cedric Whitney, Bill Knudsen and Brian VanDerElzen, for their assistance with the processing, and Terry Larrow, of the Aerospace Engineering Department, for his assistance in preparation of the test facility. They also wish to thank Professor Peter Washabaugh of the Aerospace Engineering department for checking the structural calculations. Finally, the authors wish to thank Dr Kai Sun of the University of Michigan Electron Microbeam Analysis Laboratory (EMAL) for his assistance in preparation of the electron microscope images.

References

[1] McMichael J M and Francis M S 1997 *Micro Air Vehicles—Towards a New Dimension in Flight* (Washington, DC: DARPA)
[2] Ho C M and Tai Y C 1998 Micro-electro-mechanical systems (MEMS) and fluid flows *Annu. Rev. Fluid Mech.* **30** 579–612
[3] Gad-el-Hak M 2001 The fluid mechanics of microdevices—the Freeman Scholar Lecture *J. Fluids Eng.* **121** 5–33
[4] Sun Q, Boyd I D and Candler G V 2004 A hybrid continuum/particle approach for modeling subsonic, rarefied gas flow *J. Comput. Phys.* **194** 256–77
[5] Kaplan C R and Oran E S 2002 Nonlinear filtering for low-velocity gaseous microflows *AIAA J.* **40** 82–90
[6] Martin M J, Scavazze K J, Boyd I D and Bernal L P 2006 Design of a low-turbulence, low-pressure wind-tunnel for micro-aerodynamics *J. Fluids Eng.* **128** 1045–52
[7] Sinton D 2004 Microscale flow visualization *Microfluid. Nanofluid.* **1** 1613–4982
[8] Lempert W R, Jiang N, Sethuram S and Samimy M 2002 Molecular tagging velocimetry measurements in supersonic micro jets *AIAA J.* **40** 1065–70
[9] Martin M J and Boyd I D 2006 Momentum and heat transfer in a laminar boundary layer with slip flow *AIAA J. Thermophys. Heat Transfer* **20** 710–9
[10] Sun Q, Boyd I D and Candler G V 2002 Numerical simulation of gas flow over microscale airfoils *AIAA J. Thermophys. Heat Transfer* **16** 171–9
[11] Ugural A C and Fenster S K 1995 *Advanced Strength and Applied Elasticity* (New York: Prentice Hall)
[12] Peterson K E 1982 Silicon as a mechanical material *Proc. IEEE* **70** 420–57
[13] White F M 1991 *Viscous Fluid Flow* (New York: McGraw-Hill)
[14] FLUENT/UNS User's Guide. Release 3.2. 1995 (Lebanon, NH: Fluent, Inc.)
[15] Raccurt O, Tardif F, d'Avitaya F A and Vareine T 2004 Influence of liquid surface tension on stiction of SOI MEMS *J. Micromech. Microeng.* **14** 1083–90
[16] Lide D R (ed) 2006 *CRC Handbook of Chemistry and Physics* 87th edn (Boca Raton, FL: CRC Press)
[17] Weaver W, Timoshenko S P and Young D H 1990 *Vibration Problems in Engineering* (New York: Wiley)
[18] Fang W and Wickert J A 1994 Post buckling of micromachined beams *J. Micromech. Microeng.* **4** 116–22